# Velocity measurements in a pump volute with a non-rotating impeller

**R. N. Thomas, G. J. Kostrzewsky and R. D. Flack***

A Plexiglas laboratory pump with rectangular cross sections was tested and volute velocities were measured with a laser velocimeter. First, the pump with a four bladed rotating impeller was run at three flowrates. Second, the rotating impeller was replaced with a 32-bladed non-rotating impeller with forward facing blades that imparted a swirl to the flow under forced circulation that simulated the rotating impeller case. Velocity measurements in the discharge region and flow visualization in the entire volute indicate that the proper general flow characteristics were achieved with the flow swirler but the unsteady 'jet-wake' regions were eliminated. Thus similitude was attained between the rotating and non-rotating impellers allowing study of volute flow characteristics without rotating impeller effects. Two non-rotating impellers were used to provide data for comparison to future steady state theoretical analyses. One produced a flow field that represented 121% of the nominal capacity and the other represented 160% of the nominal capacity. Detailed velocity traverses were made in the volute region for both swirlers. Circumferential non-uniformities (up to 275% from the mean) were found and were largest for the 160% simulated capacity. These are not due to rotating impeller effects and are attributed to the mismatch between the exit angle of the swirler and the volute. Radial non-uniformities in velocity were also seen (up to 22%) and the largest variations were observed for 121% simulated capacity. Finally, axial variations up to 30% were observed and these also were largest for 121% simulated capacity.

**Keywords:** *volute velocities, velocity measurement, rotating and non-rotating impellers, flow field*

The combination of boundary layer effects, coriolis acceleration, curvature, viscosity, 3-D effects and non-uniform inlet conditions makes the nature of flow in turbomachines exceedingly complex. Experimental measurements in turbomachines previously have enabled designers to improve the machines' performance immensely. In the past a major portion of the experimental results have been on the overall hydraulic performance of turbomachines; detailed local measurements exist but are not as common. As the needs for larger, more powerful and higher speed turbomachines operating under various conditions have been demonstrated, the present state of detailed knowledge requires expansion. These needs are coupled with the advancement of numerical methods and their potential in quickly solving complex flow problems.

In order to numerically model these flow problems successfully the conditions to be modelled must be identified and quantitatively understood. This understanding will aid in the development and verification of the numerical techniques. The tools available to the experimentalist have progressed from Pitot tubes to the totally non-invasive Laser Velocimeters (LV). By combining techniques the present day experimentalist can successfully quantify the different factors influencing flow in turbomachines. The objective of the present research was to isolate one of these factors for pump flows: the influence of the interaction of the impeller exit absolute flow angle with the volute angle on the local velocities. The present data will provide an effective benchmark for future steady state analyses of volute flows.

A large majority of previous research in centrifugul pumps has focused on the impeller flows. Although these flows are important in the present work, they are not of primary interest. Thus, the literature dealing solely with impeller flows will not be reviewed here for the sake of brevity. References on volute flows are below.

Some of the earliest experimental studies of flows in volutes were by Binder and Knapp[1], Bowerman and Acosta[2], and Iversen *et al.*[3]. In all three of these papers pressures were measured around the volute. At off-design conditions, non-uniformities were reported.

Csanady[4] analysed the potential flow in a logarithmic spiral volute with the aid of conformal mapping. He assumed that the total head was constant around the impeller periphery, that the tongue tip was infinitely thin, and calculated the static load on the impeller.

Worster[5] used potential flow theory to superimpose a source and a free vortex to model the flow in a volute and near the tongue. He also experimentally studied the effect of three different tongue lengths on the hydraulic performance and pressure distribution in a process pump.

* Department of Mechanical and Aerospace Engineering, University of Virginia, Charlottesville, Virginia 22901, USA
Received 3 May 1985 and accepted for publication in final form on 15 August 1985

Wesche[6] used a simple source-vortex model to theoretically study the flows in volutes with thick tongues. He examined the flow behaviour in volutes with finite size tongues and infinitely thin tongue tips.

Imaichi *et al.*[7] used an integral equation formulation to theoretically study the interaction of an impeller, volute case and tongue. They used potential flow and jet-wake flow methods to predict the unsteady flow (due to a finite number of blades) on the flow field in a centrifugal pump for two tongue shapes.

Kurokawa[8] theoretically studied frictionless flow in a 2-D logarithmic spiral volute by integrating the equations of motion. He presented velocity profiles and compared them to the data of others and also calculated the static pressure and developed force.

Carter[9] used a potential flow finite element method in the volute region and used a superposition of circulation and radial flow. He imposed a stagnation point on the tongue and solved for a circulation that produced this. The circulation was then used to calculate the flow in other parts of the volute. Carter did not consider the flow at off-design conditions.

Flack and Lanes[10] developed a transparent laboratory model pump facility to study the details of the flows in centrifugal pumps. Pump hydraulic performance was studied for different tongue clearances and positions.

Brownell and Flack[11] visualized the flow characteristics in the volute near the tongue in a centrifugal process pump. They observed the location of the stagnation point on the tongue as a function of flowrate, instantaneous blade position and rotational speed.

A series of papers has been published in which laser velocimetry has been used to measure turbomachinery flow fields[12-19]. Most of these have been for measurements in impellers in which characteristics such as jet-wake flows are measured. None has concentrated on volute flows.

As summarized in the literature, much of the previous work on pump flows has focused on overall effects of impeller/volute interactions. Namely, the total hydraulic performance and pressures are common methods of quantifying these effects. A few local velocity investigations have been performed; however, complete studies have not been performed in volutes. The overall goal of the research was to obtain a complete set of data for the velocities in a volute.

Currently, a theoretical method is not available to reliably predict the 3-D flow conditions in a pump volute with unsteady, viscous flows in which phenomena such as separation, turbulence and secondary flows occur. These phenomena are more exaggereated for off-design conditions than for on-design. As indicated above, most of the analyses that have been applied to pump volutes are potential flow methods. These do not have viscous or unsteady effects. Other 'theoretical' techniques employed use empiricism. Currently, several generic fluid mechanics computational methods are being developed for 2-D and 3-D steady and unsteady viscous flows[20,21]. These have not been applied to pumps however. To eventually accurately predict the flow conditions in any pump, theoretical methods must be verified with benchmarks. One will not be able to consider the 3-D unsteady viscous flow conditions in an actual pump as the first verification step. One will need to check simple methods and geometries first and expand the methods to more complex situations. For example, if one cannot predict the steady flow situation, one should not expect to be able to reliably predict unsteady flow. The rig built for the current research is intended to be a benchmark for 3-D viscous steady-state flow predictions. Eventually, experimental data from the same rig will be published to include unsteady effects.

The first specific objective of the research was to remove the rotational effects of the impeller and provide an inlet flow with a uniform flow angle to the volute. This allows the velocity field in the volute to be mapped out, with the use of a LV, without the complexities associated with a rotating impeller. These complexities include the so-called jet-wake flow structure and associated blade pass frequencies, inlet pre-rotation, and centripetal accelerations. This will provide a 3-D steady-state benchmark and aid in the development of numerical models by simplifying the problem to be solved. By advancing one step at a time, fully understanding the fundamental fluid flow involved at each step, and verifying the different theoretical prediction methods at each step the complete 3-D viscous and unsteady flow problem can eventually be solved.

The second specific objective was to experimentally determine the effect of the impeller exit flow angle on the velocity distribution. As was noted in previous literature, an asymmetric circumferential distribution of flow gives rise to a force on the impeller, which in turbomachines can become quite large and destructive. By simulating off-design conditions, a means of quantifying the asymmetric distribution is achieved. The distribution can later be compared with the results for the rotating impeller to determine the unsteady and rotational effects, if any, on the radial distribution.

For the present research the pump described in Ref 10 was modified by replacing the rotating

## Notation

$c_m$ Radial velocity at impeller exit (Fig 6)
$D$ Impeller diameter
$Q$ Volumetric flowrate
$r$ Radial position
$r_i$ Impeller radius $= D/2$
$r_v$ Volute radius at a particular $\theta$
$\bar{r}$ Non-dimensional radius $= (r - r_i)/(r_v - r_i)$
$t$ Passage axial thickness
$U$ Impeller tip velocity (Fig 6)
$V$ Absolute velocity
$V_r$ Radial velocity
$\bar{V}_r$ Average radial velocity at impeller exit
$V_t$ Tangential velocity
$V_v$ Vertical velocity
$x$ Horizontal position in discharge region (Fig 3)
$z$ Axial position relative to volute centreplane
$\alpha_2$ Ideal absolute flow angle
$\alpha'_2$ Actual absolute flow angle (Fig 6)
$\beta_2$ Ideal flow angle relative to rotating impeller
$\beta'_2$ Actual flow angle relative to rotating impeller (Fig 6)
$\theta$ Circumferential position (Fig 3)
$\lambda$ Volute angle

impeller with a swirl generator. Two simulated capacities were studied and velocity traverses in the radial, circumferential, and axial directions were performed. Two components of velocity (in the plane of the volute) were measured around the volute.

## Apparatus

The centrifugal pump was operated in two modes. First, the pump had a conventional rotating impeller. Second, the pump facility was modified to obtain measurements with a stationary 'impeller' in place of the rotating impeller. This stationary impeller or 'swirl generator' was used to simulate flow conditions in a pump by matching the flow angle of the fluid exiting from the swirl generator to the average flow angle of fluid exiting from a rotating impeller. A laser velocimeter was used to measure velocities in the volute of both systems. The following is a detailed description of the impellers, supporting apparatus and instrumentation.

### Rotating impeller test rig

The pump used for these studies is fully documented in Ref 10 and a schematic of the volute and impeller is presented in Fig 1. Important details of the pump are described herein.

The pump was designed using 2-D theory to operate nominally at 0.0037 $m^3/s$ (59 gpm). It uses a 4-bladed, fully-shrouded Plexiglas impeller with a diameter, $D$, of 203.2 mm (8.00 in). The impeller blades are log-spirals with a constant vane angle ($\beta_2$) of 16°. The nominal design absolute exit flow angle ($\alpha'_2$) from the impeller is 7°. The flow channel depth, $t$, of the impeller and of the entire pump is 12.7 mm (0.5 in). The volute has a log spiral shape with a spiral angle $\lambda = 83°$. The increasing radius of the volute is given by $r_v = 0.108\, e^{0.115(\theta - 0.1145)}$ metres, where $\theta$ is in radians. The tongue is located 7° above the centre of the impeller, thereby producing a tongue clearance to the impeller periphery of 6.3 mm (0.25 in).

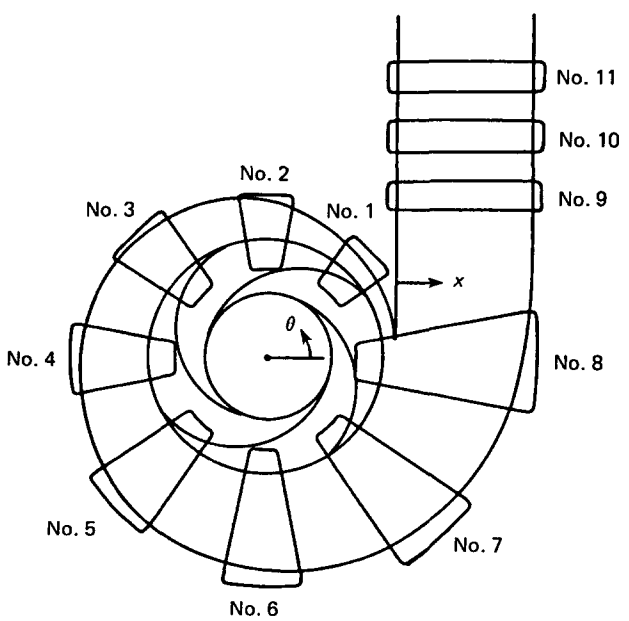


*Fig 1 Volute and rotating impeller with LV access windows*

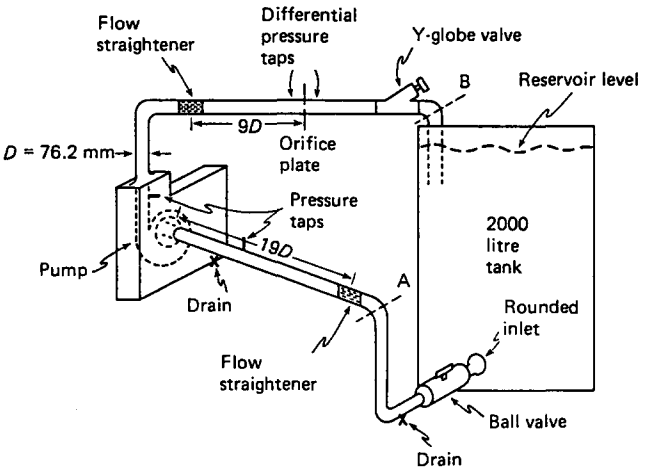


*Fig 2 Closed loop test facility*

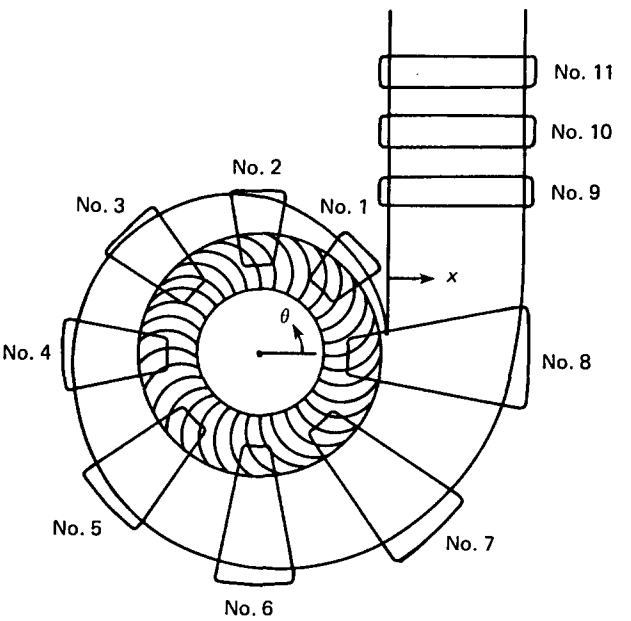


*Fig 3 Volute and 32-blade stationary 'Swirl generator'*

The pump is in a conventional closed loop water system as shown in Fig 2. It is driven at 619 r/min by a 0.5 hp electric motor and toothed belt pulley system. The speed did not vary by more than 3 r/min for all of the tests. The inlet and exit water temperatures were 19°C for all of the tests. The flow rate was measured with an orifice meter.

To facilitate LV measurements and maintain sufficient strength, recesses were machined into the front and rear housings as shown in Fig 1. LV measurements were made in these 9.5 mm thick 'windows'.

### Stationary impeller test rig

The system described above was modified to accommodate a stationary impeller. Now, the pump was not used in a pump mode, but as a static test facility. As indicated earlier, the rotating impeller was replaced with a stationary element to induce a swirl to the flow. The general schematic is shown in Fig 3.

Two modifications were made. First, the 32-blade Plexiglas impeller having the same dimensions as the rotating impeller was attached to the shaft and the shaft

was immobilized. The second modification was to connect the static test facility to a gravity fed constant-head water circulation system. The test loop in Fig 2 was modified at sections A and B and spliced into the constant head facility. The overall constant-head system is diagrammed in Fig 4. This system uses a 3.0 $m^3$ constant-head supply tank located 10 m above the test rig. Water flows from the supply tank, through the test rig and into a sump tank where return flow to the supply tank is provided by two pumps connected in parallel. All piping is 76.2 mm (3.0 in) ABS.

Two different stationary swirl generators were used. Each had 32 blades to produce uniform flow circumferentially. The exit blade angles ($\alpha_2$) of the two swirlers were 4° and 16°. Due to 'slip', the fluid exiting the swirlers was at angles ($\alpha'_2$) of 10° and 20° respectively for the two swirlers. The first represents 121% of the nominal flow rate while the second represents 160% of this flow. This will be discussed later.

The 32 blades of each stationary impeller generated a flow of uniform flow angle. For the case with $\alpha_2 = 4°$ the maximum flow angle deviation was 0.9° around the periphery. The conditions with $\alpha_2 = 16°$ produced a maximum deviation of 2.2°. This difference was attributed to the larger exit area for the case with $\alpha_2 = 16°$ and hence the fluid was not confined to the blade passages as well.

## Laser velocimeter system

A brief description of the LV is presented here. The general layout of the LV is shown in Fig 5. The system is a one-directional forward scatter dual beam LV. The entire optical package (transmitting and receiving optics) is mounted on one mill table so that optical alignment was maintained throughout the tests. The location of the probe volume (where the measurements are obtained) was positioned in all three directions by traversing the mill bed. The uncertainty in position is 0.2 mm.

The wavelength used is 488 nm. The beam is split into two equal intensity components by a beam splitter.

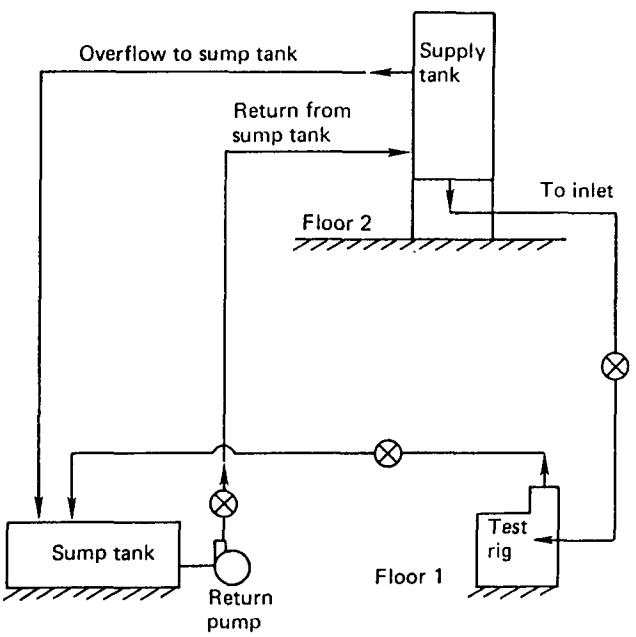


*Fig 4 Constant-head test loop*

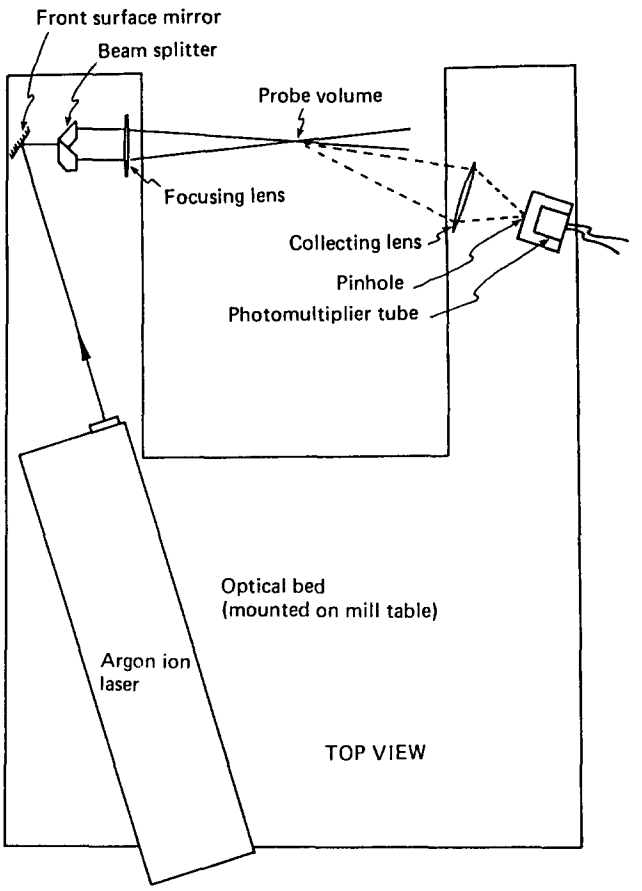


*Fig 5 Forward scatter LV system*

Although the LV system is one-directional, at each point in the flow at least two directions were measured by rotating the beam splitter and laser head in separate tests.

The sending (or focusing) lens and collecting lens have focal lengths of 305 mm and 50 mm, respectively. This results in a probe volume 146 μm in diameter and 1780 μm long. The light scattered by particles in the flow is focused onto a 179 μm pinhole in front of a photomultiplier tube. The output of the PMT is high-pass filtered, amplified and sent to a signal processor.

The signal processor is a burst type processor with two important validity checks. First, the amplitude of the Doppler signal must exceed a minimum noise threshold and remain below a maximum overload to ensure that the signal is not noise. Second, a 5- and 8-count comparator is used to reject signals for multiple particles in the probe volume. Each valid signal is stored with a dedicated minicomputer and data analysis is performed after each test was completed.

To obtain LV signals of good quality, appropriate particle seeding in the flow must be present. Microscopic investigations indicated that tap water, after being filtered (using an odour and taste filter), contained particles 3 μm and less in diameter and of suitable scattering properties. The water in both test facilities (non-rotating and rotating) was filtered upon initial filling and then periodically recirculated through the filters. Valid signals with high visibilities were achieved using this method.

Radial traverses in the volute region at six locations around the stationary impellers were taken. These locations are identified by window numbers and circumferential angle, $\theta$. In addition to these six

circumferential locations, traverses in the pump discharge region were made.

Velocity measurements at each of these positions for three flow rates were made. At each of the radial positions, the probe volume was initially positioned approximately 4 mm from the exit of the impeller. The probe volume was then moved radially outward to the volute wall for other data positions. The number of separate data points taken for a radial traverse was dependent upon the circumferential angle, $\theta$. At each data position, 500 velocity samples were recorded. This ensured that the mean velocity and other statistical characteristics of the data point were accurately represented. At each data position orthogonal sets of velocity data were collected. The directions of the two velocity sets were approximately $\pm 45°$ to the mean flow direction. Typical uncertainties in the absolute velocities were 2.4% and the flow angles were uncertain to $\pm 2.3°$.

In addition to the circumferential and radial traverses, axial traverses were performed at some positions. For each of the axial traverses five velocity sets were obtained.

LV measurements were also attempted for the pump with the rotating impeller. However, due to blade passing jet-wake regions, large fluctuations in the velocities existed in the volute region. Thus, it was not possible to accurately high-pass filter the high frequency components (Doppler frequency) while removing the low frequency component (pedestal frequency) from all of the signals, which is necessary for further signal processing. This problem can be and has since been eliminated with the addition of frequency shifting to the LV system. For the present paper LV measurements were made in the discharge regions where much of the blade pass fluctuations had dissipated.

## Flow visualization

Flow visualization was also used to indicate the qualitative similitude of the pump with the stationary swirler and the pump with the rotating impeller. Small air bubbles were injected into the flow through the static pressure tap located on the inlet piping 0.6 m from the test rig using an electric air pump. The bubbles were too large for accurate quantitative measurements to be made. The primary purpose was to locate the streamlines, stagnation points, and areas of separation around the tongue and in the discharge. Time exposure photographs were taken of the volute, tongue, and discharge regions at various flow rates using a 35 mm camera.

# Similitude

As indicated earlier, two stationary 'impellers' or swirlers were used to simulate the flow exiting from a rotating impeller. The first objective is to demonstrate that the two different swirlers that were used simulated the ideal flow (ie no blade pass fluctuations) at 121% and 160% of the nominal design flow rate. This is accomplished first by an examination of the velocity triangles and second by flow visualization near the tongue.

The exit velocity triangle for the rotating impeller at the nominal design flow rate is shown in Fig 6. The average absolute flow angle, $\alpha_2'$, is 7.0 and the average radial velocity is 0.457 m/s. Also, the flow angle relative to

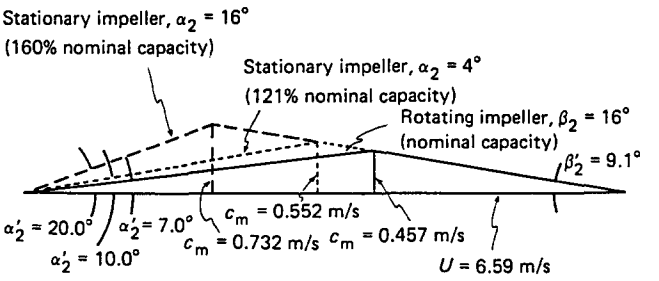


*Fig 6 Exit velocity triangles*

the impeller ($\beta_2'$) is 9.1° which is lower than the 16° blade angle due to slip.

For the stationary impeller with $\alpha_2 = 4°$ the average absolute flow angle ($\alpha_2'$) at the exit of the impeller was measured with the LV to be 10°. The exit velocity triangle is also shown in Fig 6 for this case. The mean radial velocity is now 0.552 m/s or 121% of the nominal capacity.

Finally, the average absolute flow angle for the second stationary impeller ($\alpha_2 = 16°$) was measured to be 20°. This also is shown on Fig 6. For this angle the average radial velocity is 0.732 m/s (160% nominal capacity).

The uniformity of the flow around the exit of the swirler was also checked. The probe volume was positioned at the tip of a blade and the velocity and flow angle were measured. The probe volume was then moved to a position in the centre of the impeller passage between blades and the measurements recorded. By performing these tests around the swirler and comparing the measurements, it was determined that a uniform exit flow angle was present around the swirler and between all blade passages.

Measurements with the LV were made at three flow rates for the stationary impellers and the exit flow angle ($\alpha_2'$) was the same for all flow rates. Thus, these flow rates all represent the *same* simulated percent capacity. The stationary impellers fix the absolute flow angle and this angle did not change with flow rate as it does in a rotating impeller. The change in flow rates through these stationary impellers is analogous to changing the rotational speed in a real pump while holding all the non-dimensional pump characteristics constant.

Flow visualization was also used to determine the similitude of the pump with the rotating impeller and stationary swirler. Typical results are presented in Fig 7 for flows near the tongue. Streamlines are shown in Fig 7(a) for 127% capacity with the rotating impeller in the pump. As can be seen, the stagnation point is on the inside of the tongue and a separation zone is present on the outside of the tongue. Streamlines for the stationary impeller ($\alpha_2 = 4°$) and 121% simulated flow rate are shown in Fig 7(b). Once again, the stagnation point is on the inside of the tongue and a separation zone occurs on the discharge side of the tongue. By comparing Figs 7(a) and (b) one can see that the flow angles and patterns are qualitatively the same for the two tests at approximately the same flow capacity.

Other flow rates were tested as well and streamlines were found in other portions of the volute. These results are not presented for the sake of brevity and because Brownell and Flack[11] found that the streamline patterns near a tongue change more than streamline patterns elsewhere in a volute with changes in flow

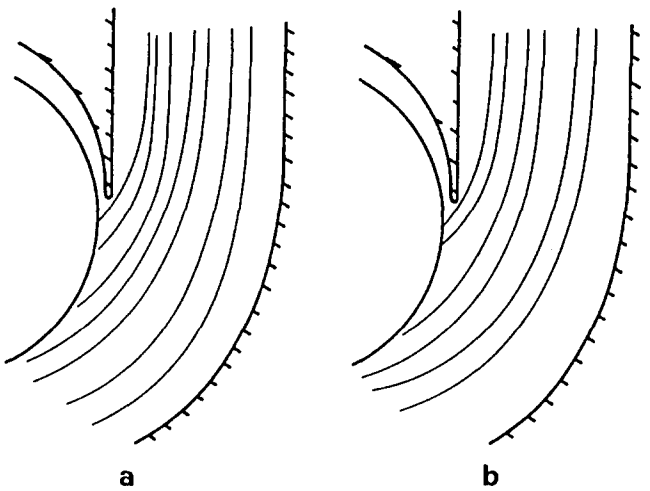


*Fig 7 Streamlines for: (a) Rotating impeller at 127% capacity. (b) Stationary impeller ($\alpha_2 = 4°$) at 121% simulated capacity*

conditions. At low flow rates the stagnation point was on the discharge side of the tongue. When the percent flow rates were matched, the streamlines were always similar for the two pump configurations over all portions of the volute. Brownell and Flack[11] performed similar studies in the tongue region of an industrial process pump. They found that the stagnation point on the tongue changed positions with flow rate qualitatively the same as found here.

Thus, two studies were presented in this section. They showed that the pump with the simulated impeller flow was accurately producing flows without jet wake characteristics, representing 121% and 160% nominal capacities for a pump with a rotating impeller. In the next section detailed velocity measurements will be presented.

## Results

Described earlier, laser velocimeter measurements were made in the volute and discharge regions. In this section typical results will be presented.

### Discharge region

Results are presented for flows in the discharge region (window 10) for the pump with the rotating impeller. In Fig 8 profiles for the vertical velocity component at the axial centreline of the pump are presented. Profiles were obtained for three flow rates representing 59%, 100% and 127% of the nominal capacity. At 59% capacity the profile is uniform to within 10% of the mean. However, at 127% capacity the velocity varies by 60% of the mean. It is important to note that Flack and Lanes[10] found that the peak efficiency of the pump occurred at 59% of the nominal capacity. Flow visualization showed that the flow was not separated in this window under these conditions. However, at 127% capacity flow near the wall is approaching separation since the velocity is low.

Velocity profiles for the non-rotating impeller with $\alpha_2 = 4°$ (121% simulated capacity) in the discharge region (window 10) are shown in Fig 9. Three flowrates were tested and separation was not observed for any of the cases. The velocities were also non-dimensionalized by the average radial velocity out of the impeller ($\bar{V}_r = Q/\pi tD$) and plotted in Fig 10. The profiles all collapse to one curve within the experimental uncertainty indicating similitude among the three cases.

These non-dimensionalized profiles are also compared to the non-dimensionalized profile for the case of the rotating impeller at 127% capacity in Fig 10. As can be seen, all profiles have essentially the same shapes. They are the same within experimental uncertainty and are moderately skewed towards the outer volute wall. Thus, the data in Fig 10 complement the discussion and figures in the previous section on similitude. This figure also indicates that the pump operating with the rotating impeller and flow swirler displays the same characteristics for both.

Results for $\alpha_2 = 16°$ (160% simulated flow) are shown in Fig 11. Once again three flowrates were tested

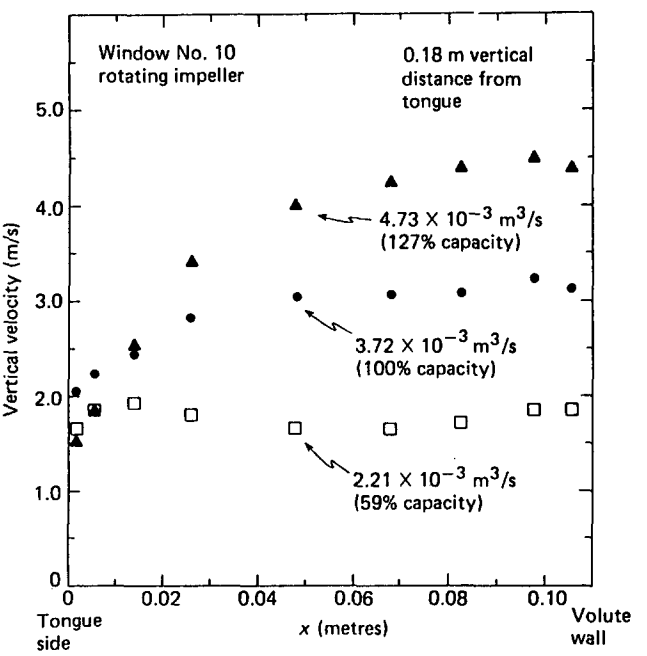


*Fig 8 Velocity profiles in discharge region with rotating impeller*

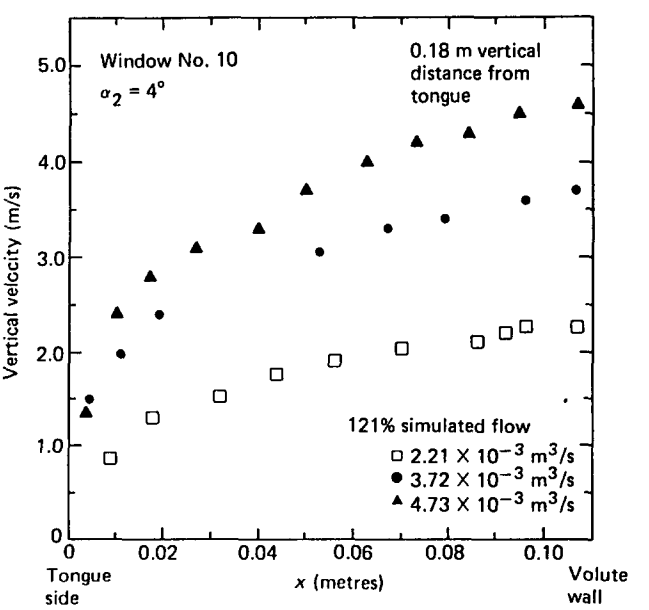


*Fig 9 Velocity profiles in discharge region with stationary impeller ($\alpha_2 = 4°$, 121% simulated capacity)*

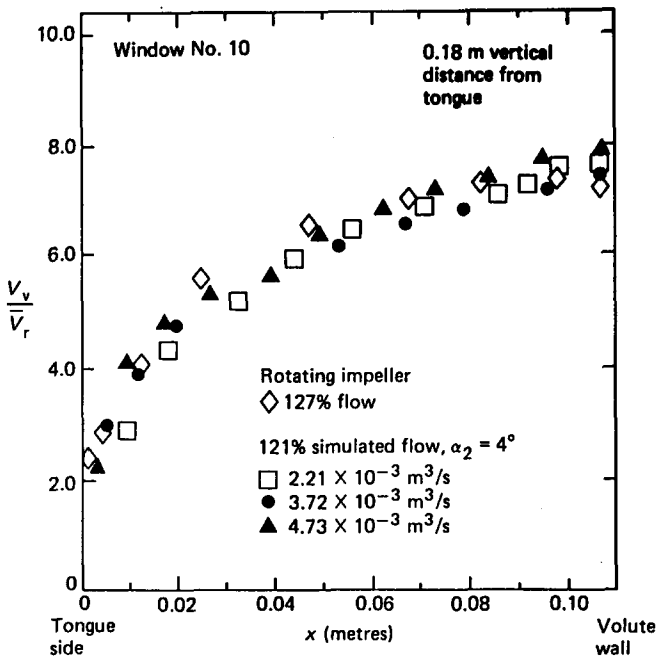


*Fig 10 Non-dimensionalized velocity profiles in discharge region with rotating (127% capacity) and stationary (121% simulated capacity) impellers*

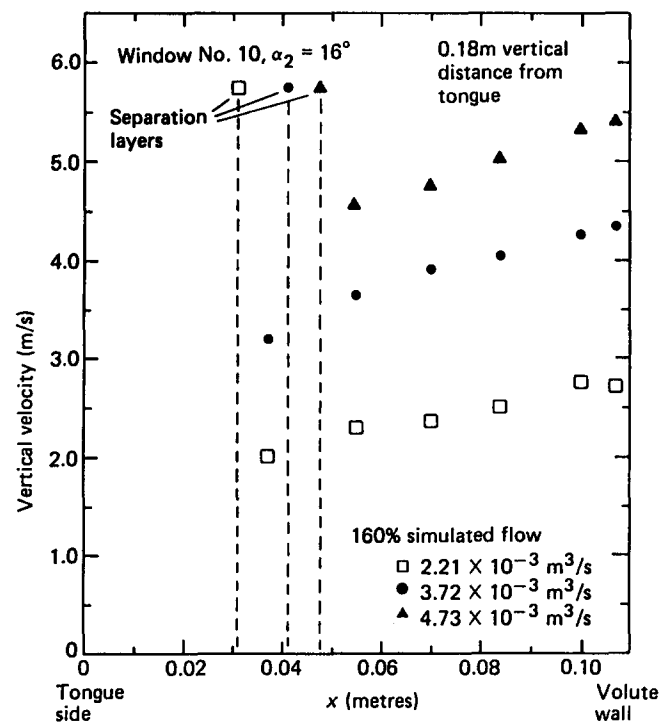


*Fig 11 Velocity profile in discharge region with stationary impeller ($\alpha_2 = 16°$, 160% simulated capacity)*

and all were similar when non-dimensionalized. For this high capacity the velocity profiles are highly skewed towards the outer volute wall and separated regions were observed. These zones are shown in Fig 11.

## Volute region

A series of tests was performed on the pump with the non-rotating impeller in all of the windows in the volute region as shown in Fig 3. Radial, circumferential, and axial traverses were performed. However, only representative results will be presented herein.

**Absolute velocity profiles and flow angle profiles in the radial traverse for $\alpha_2 = 4°$ and $\theta = 142°$ are presented in Fig 12. The velocity profiles are from the impeller tip to the volute wall and flow angles for the absolute velocity are measured relative to the circumferential direction. Results are presented for three flowrates and at the axial centreplane. The flow angle is approximately 10° at the impeller exit, reaches a maximum value of approximately 18° midway between the exit and wall before returning to 7° at the volute wall. The flow angles are independent of flowrate. The largest velocities are observed at the impeller exit.**

Non-dimensionalized profiles in the radial direction for the axial centreplane are presented in Fig 13 for $\alpha_2 = 4°$ and $\theta = 142°$. Once again similitude is observed. Also in Fig 13 the non-dimensionalized absolute velocity radial profile is shown for $\alpha_2 = 16°$ (160% simulated capacity) and $\theta = 144°$. By comparing results for $\alpha_2 = 4°$ and 16° two trends can be seen. First, the profile is more radially uniform at high simulated flowrates. For example, at 121% capacity a variation of 16% from the mean is seen, whereas at 160% capacity a variation of 7% is noted. Second, at $\theta \simeq 142$–144° the measured non-dimensionalized axial centreplane velocities are higher at low simulated flowrates.

Although a figure is not presented, the radial profile of the flow angle for $\alpha_2 = 16°$ at $\theta = 144°$ will be

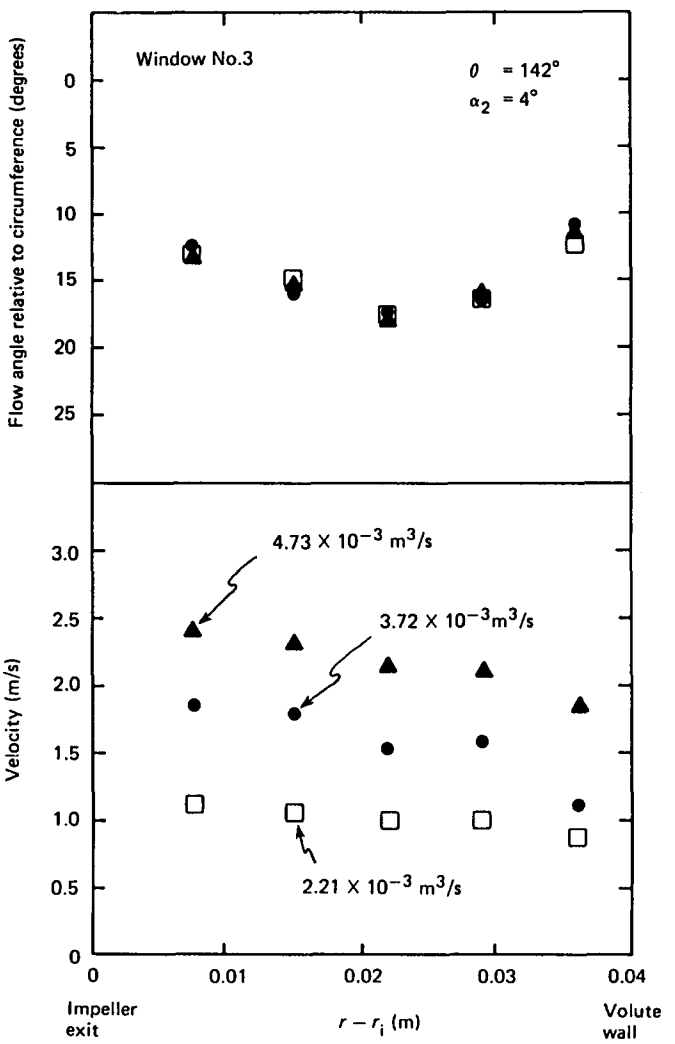


*Fig 12 Radial profiles of absolute velocity and flow angle at $\theta = 142°$ ($\alpha_2 = 4°$, 121% simulated capacity)*

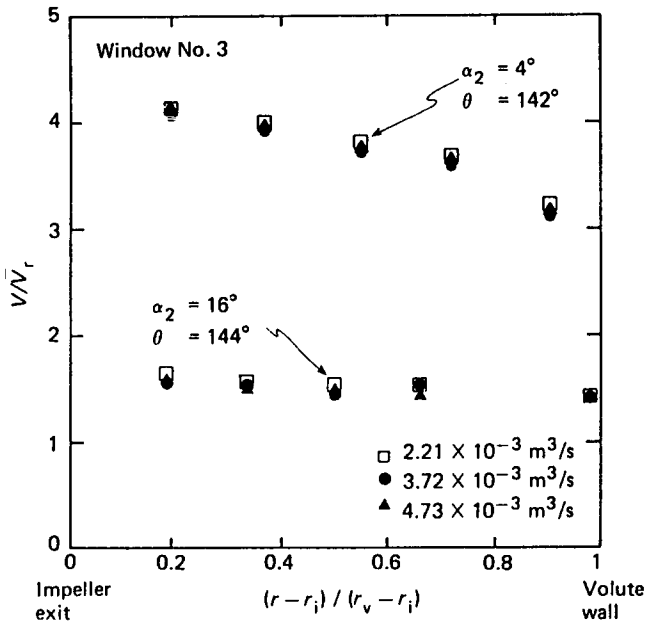


*Fig 13 Non-dimensional radial profiles of absolute velocity for $\alpha_2=4°$ (121% simulated capacity) and $\alpha_2=16°$ (160% simulated capacity) at $\theta\simeq142$–144°*

discussed. For this case the flow angle was approximately 20° at the impeller exit, increased to 22° at mid channel, and reduced to 7° at the volute wall. It is worthy to mention that the radial variation of velocity for this case was less than for $\alpha_2=4°$ (Fig 12).

Non-dimensionalized absolute velocity radial profiles in the axial centreplane are presented in Fig 14 for $\alpha_2=4°$ and $\alpha_2=16°$ at $\theta\simeq311$–312°. The same two trends persist at this circumferential position. Namely, the profile is more uniform at high simulated flow rates (18% variation) than at low simulated flow rates (22% variation) and the centreplane value is largest for the low simulated flow rate. Also, for both values of $\alpha_2$, the velocity amplitudes are larger at $\theta\simeq311$–312° than at 142–144°.

Thus far only the velocity in the axial centreplane has been discussed. In Fig 15 the axial profiles for the absolute velocities for $\alpha_2=4°$ at $\theta=312°$ and at three radial locations are presented. The non-dimensional radial positions ($\bar{r}$) are: 0.081, 0.288 and 0.977. Once again, three flowrates were used and similarity was attained. Overall, the profiles are relatively flat except near the impeller. Near the impeller the peak velocity is 28% higher than the average velocity. At other circumferential positions for $\alpha_2=4°$, similar trends were observed. Namely, the maximum flow near the impeller was higher than the average by 26 to 30% while the profiles were uniform at non-dimensional radial positions of 0.3 and larger. For $\alpha_2=16°$ the peak velocity was typically 10% higher than the average near the impeller. At non-dimensional radial positions of 0.3 and larger the profiles were once again nearly uniform.

To summarize some of the results Figs 16 and 17 are presented. These two figures are circumferential profiles of the non-dimensionalized tangential and radial velocities at the impeller periphery and in the axial centreplanes for $\alpha_2=4°$ and 16°. As can be seen, the profiles are highly non-uniform. Low velocities are seen for small values of $\theta$ (near the tongue). The profiles for $\alpha_2=4°$ are more uniform than those for $\alpha_2=16°$. For example, data for the radial velocity for $\alpha_2=4°$ varies by as much as 150% from the mean of the centreplane velocities whereas the data for $\alpha_2=16°$ varies by as much as 275% from the mean. The highest velocities always occur in the volute near the discharge (either window no 7 or 8).

It is important to note that these circumferential non-uniformities occur solely due to an interaction between the steady flow and the volute geometry. Namely,

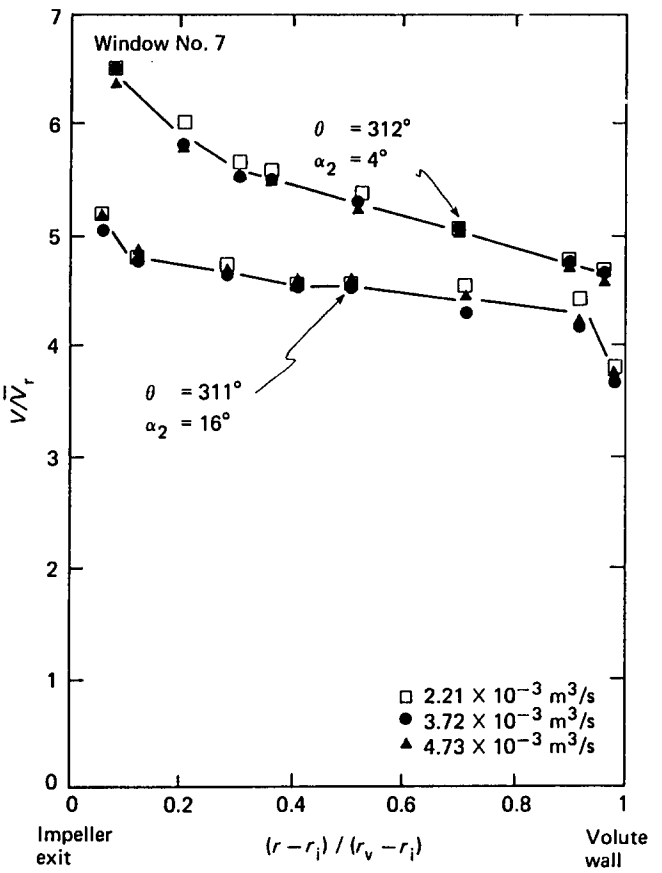


*Fig 14 Non-dimensional radial profiles of absolute velocity for $\alpha_2=4°$ (121% simulated capacity) and $\alpha_2=16°$ (160% simulated capacity) at $\theta\simeq311$–312°*

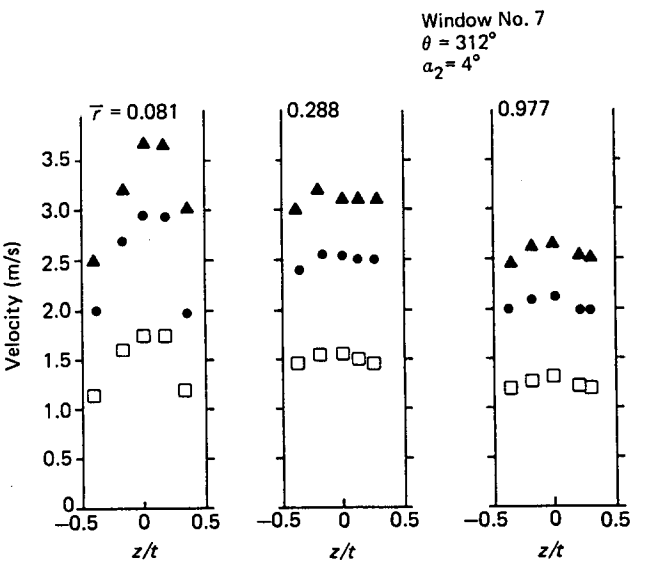


*Fig 15 Axial profile of absolute velocity at $\theta=312°$ and three radial positions ($\alpha_2=4°$, 121% simulated capacity)*

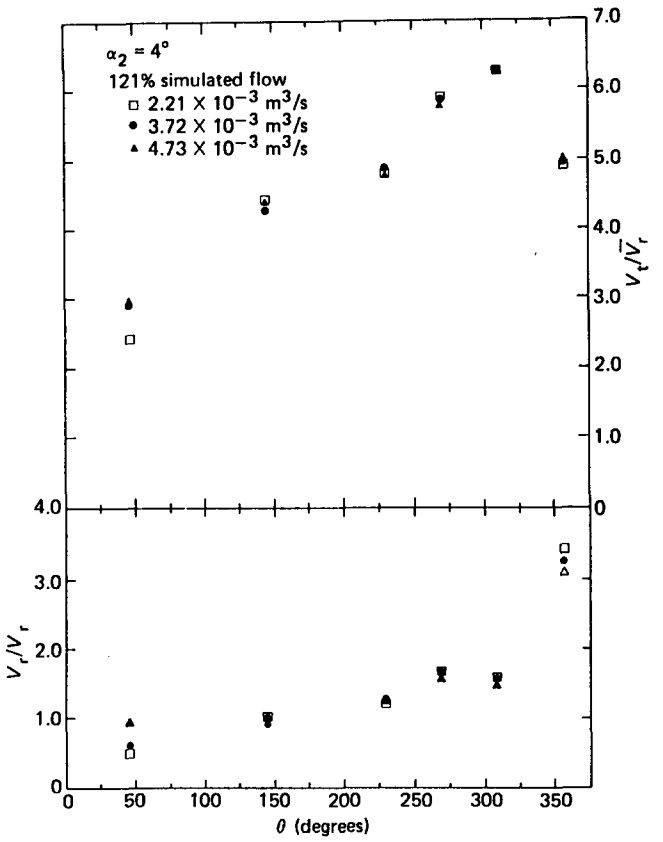


*Fig 16 Non-dimensional circumferential profiles of radial and tangential velocities at impeller exit ($\alpha_2 = 4°$, 121% simulated capacity)*

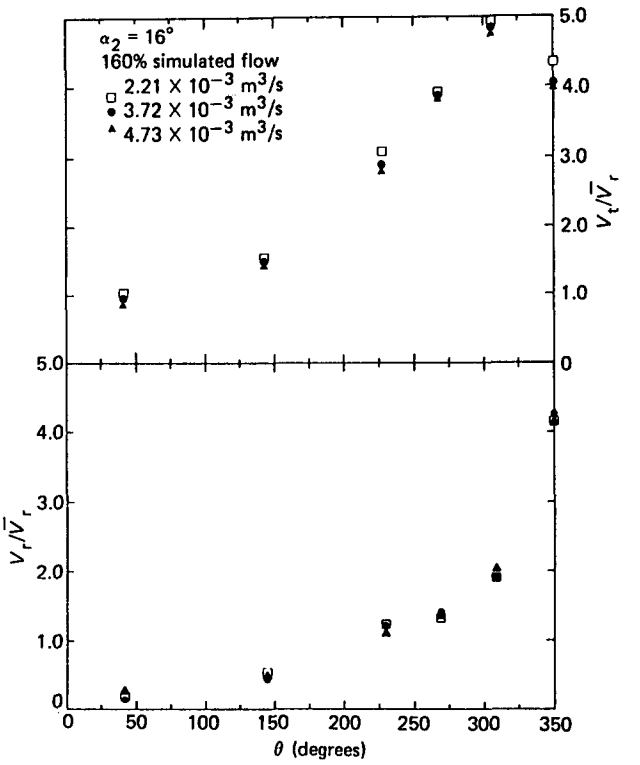


*Fig 17 Non-dimensional circumferential profiles of radial and tangential velocities at impeller exit ($\alpha_2 = 16°$, 160% simulated capacity)*

since the impeller was not rotating, complex unsteady interactions due to blade passing which could cause non-uniformities were eliminated. The non-uniformities are due to a mismatch between the flow exiting the swirler and the volute shape.

As a final evaluation of the data, the non-dimensional radial velocities were integrated in the axial and circumferential directions and divided by $\pi tD$ to find the measured average non-dimensional radial velocity from LV data. For both cases ($\alpha_2 = 4°$ and 16°) this average radial velocity was found to be 1.02 which is only 2% higher than the ideal value and well within the experimental uncertainty.

## Summary

Extensive LV measurements were obtained in the volute region of a centrifugal pump for two non-rotating impellers. These two stationary impellers simulated ideal flows generated by the rotating impeller at 121% and 160% nominal design capacity. Measurements in the discharge region of the pump, with the rotating impeller in place, at 59%, 100% and 127% nominal design capacity were also made. One of the major objectives of the research was to provide experimental data for future steady state analyses of volute flows. The conclusions can be summarized as follows:

1) The principal objective of effectively removing the rotational effects while preserving the general characteristics of pump flow was achieved. General flow patterns for the case of 121% simulated capacity were the same as those for the case of 127% actual capacity as observed with flow visualization. Also, velocities in the discharge region for the two cases were the same. Thus, similitude was attained with the non-rotating impellers.

2) The flows with the stationary impellers represented the general characteristics of off-design pump operation. These characteristics were separation off the tongue for both cases and an asymmetric circumferential distribution of velocities at the impeller periphery. For example, for 121% simulated flow the deviation of the radial velocity was as high as 150% from the average while at 160% simulated flow the deviation was as high as 275%.

3) For the pump volute flow studied here, the further from design conditions that one operated the system, the more non-uniform the flow became. Thus, the circumferential non-uniformity of the flow in the volute is due to the non-rotational effects of the geometric mismatching of flow angle at the impeller exit and the volute angle. It is not due to rotational effects from an impeller.

4) The radial traverses revealed an absolute velocity profile which was not uniform for both simulated flow cases. The highest velocity was at the exit of the 'impellers' and this decreased to the volute wall. The non-uniformity was typically on the order of 30% from the average velocity.

5) For 121% simulated capacity the flow angle at the impeller exit was 10° and reached a typical maximum of 18° in the centre of the volute channel before closing up to the volute angle of 7°. For the 160% simulated capacity the flow angle at the impeller exit was typically 20° which opened up by 2° at the centre before closing down to 7°.

6) Axial traverses for the stationary impeller cases showed velocity deviations from the mean of up to 30% at the impeller exit, decreasing to 5% at centre channel.

## Acknowledgements

The work detailed in this article was sponsored in part by the NASA-Lewis Research Center under Contract No NAG3-180 and in part by the ROMAC Industrial Research Program at the University of Virginia.

## References

1. **Binder R. C. and Knapp T. R.** Experimental Determinations of the Flow Characteristics in the Volutes of Centrifugal Pumps. *Trans. ASME, 1936,* **58**, *649–661*
2. **Bowerman R. D. and Acosta A. J.** Effect of the Volute on Performance of a Centrifugal-Pump Impeller. *Trans. ASME, 1957,* **79**(*5*), *1057–1069*
3. **Iversen H. W., Rolling R. E. and Carlson J. J.** Volute Pressure Distribution, Radial Force on the Impeller, and Volute Mixing Losses of a Radial Flow Centrifugal Pump. *J. of Engineering for Power, Trans. ASME, April 1960,* **82**(*2*), *136–144*
4. **Csanady G. T.** Radial Forces in a Pump Impeller Caused by Volute Casing, *J. of Engineering for Power, Trans. ASME, October 1962,* **84**(*4*), *337–340*
5. **Worster R. C.** The Flow in Volutes and its Effect on Centrifugal Pump Performance. *Proceedings of the Inst. of Mechanical Engineers, 1963,* **177**(*31*), *843–875*
6. **Wesche W.** Designing Pump Volutes with Thick Casing Tongues. *Sulzer Technical Review, 1980,* **4**, *157–161*
7. **Imaichi K., Tsujimoto Y. and Yoshida T.** A Two-Dimensional Analysis of the Interaction Effects of Radial Impeller in Volute Casing. *1980 IAHR-AIRH Symposium, Tokyo, Japan, 635–647*
8. **Kurokawa J.** Theoretical Determinations of the Flow Characteristics in Volutes, *1980 IAHR-AIRH Symposium, Tokyo, 623–634*
9. **Carter D.** A Finite Element Analysis of Ideal Flow in a Centrifugal Pump Volute. *M.S. Thesis, University of Virginia, May 1981*
10. **Flack R. D. and Lanes R. F.** Effects of Volute Geometry and Impeller Orbit on the Hydraulic Performance of a Centrifugal Pump. *Performance Characteristics of Hydraulic Turbines and Pumps, ASME Publication H00280, 1983, 127–133*
11. **Brownell R. B. and Flack R. D.** Flow Characteristics in the Volute and Tongue Region of a Centrifugal Pump. *ASME Paper No. 84-GT-82, 1984*
12. **Eckardt D.** Instantaneous Measurements in the Jet/Wake Discharge Flow of a Centrifugal Compressor Impeller. *J. of Engineering for Power, Trans. ASME, July 1975,* **97**(*3*), *337–346*
13. **Schodl R.** A Laser-Two Focus (L2F) Velocimeter for Automatic Flow Vector Measurements in the Rotating Components of Turbomachines. *J. of Fluids Engineering, Trans. ASME, December 1980,* **102**(*4*), *412–419*
14. **Adler D. and Levy Y.** A Laser-Doppler Investigation of the Flow Inside a Backswept, Closed, Centrifugal Impeller. *J. of Mechanical Engineering Science, 1979,* **21**(*1*), *1–6*
15. **Howard J. H. G., Mukker O. S. and Naoem T.** Laser Doppler Measurements in a Radial Pump Impeller. *Measurement Methods in Rotating Components of Turbomachinery, ASME Publication 100130, 1980, 113–138*
16. **Kannemanns H.** Radial Pump Impeller Measurements Using a Laser Doppler Velocimeter. *ASME Paper No. 80-GT-94, 1980*
17. **Fister W., Zahn G. and Tasche J.** Theoretical and Experimental Investigations About Vaneless Return Channels of Multi-Stage Radial Flow Turbomachines. *ASME Paper No. 82-GT-209, 1982*
18. **Krain H.** A Study on Centrifugal Impeller and Diffuser Flow. *J. of Engineering for Power, Trans. ASME, October 1981,* **103**(*4*), *688–697*
19. **Kostrzewsky G. J.** Design, Construction and Testing of a Laser Velocimeter for Use with a Plexiglas Centrifugal Pump. *M.S. Thesis, University of Virginia, August 1982*
20. **Hah C.** A Navier Stokes Analysis of Three-Dimensional Turbulent Flows Inside Turbine Blade Rows at Design and Off-Design Conditions. *J. of Engineering for Gas Turbines and Power, Trans. ASME. April 1984,* **106**(*2*), *421–429*
21. **Rhie C. M., Delaney R. A. and McKain T. F.** Three Dimensional Viscous Flow Analysis for Centrifugal Impellers. *AIAA Paper No. 84-1296, 1984*

# BOOK REVIEW

## Potential Flows: Computer Graphic Solutions

Robert H. Kirchhoff

This admirable little book contains accurate plots of streamlines and velocity contours for 70 potential flows, 8 axisymmetric and the rest two-dimensional. It begins with a simple outline of potential flow theory, in terms of the stream function, velocity potential and complex potential, and the solutions for each flow are outlined in enough detail for a student to be able to fill in the gaps without difficulty. A few sample computer programs are given at the end.

Most lecturers in fluid dynamics will want to recommend this book to their students (the rest will merely crib it for their lecture notes). The style is so clear that it could be used as a teach-yourself book for specialists such as meterologists who have only a peripheral interest in potential flow: it can be warmly recommended to broaden the minds of mathematical students of potential theory.

The programs are directly usable only with a Hewlett Packard desk computer and plotter: one hopes that computer graphics protocols will become more standardized by the time the second edition appears, but if the book achieves the popularity it deserves this will not be long.

P. Bradshaw
Imperial College,
London SW7

Published, price $54.00, by Marcel Dekker Inc, 270 Madison Avenue, New York, NY 10016, USA, 293 pp.